Theor Chem Acc (2012) 131:1260
DOI 10.1007/s00214-012-1260-5

REGULAR ARTICLE

Theoretical study of chemosensor for fluoride anion and optical properties of the derivatives of diketopyrrolopyrrole

Ruifa Jin

Received: 7 April 2012 / Accepted: 11 July 2012 / Published online: 27 July 2012

Abstract The interactions between chemosensors, diketopyrrolopyrrole (DPP) derivatives, and different halides (F^-, Cl^-, and Br^-) anions have been theoretically investigated using DFT approaches. Theoretical investigations have been performed to explore the optical, electronic, charge transport, and stability properties of DPP derivatives as charge transport and/or luminescent materials. It turned out that the unique selectivity of DPP derivatives for F^- is ascribed to their ability of deprotonating the host sensors. The atoms in molecules theory and natural bond orbitals charge analysis of the complexes consisting of DPP derivatives and X^- (X = F, Cl, and Br) confirm that the protons are almost completely abstracted by F^-. The study of substituent effects suggests that all the substituted derivatives are expected to be promising candidates for ratiometric fluorescent fluoride chemosensors as well as chromogenic chemosensors. Furthermore, the derivatives with biphenyl, 2-(thiophen-2-yl)thiophene, and benzo[d]thieno[3,2-b]thiophene fragments are expected to be promising luminescent materials. In addition, derivatives with 2-(thiophen-2-yl)thiophene and 4,9-dihydrothieno[3,4-b]quinoxaline fragments can serve as good electron transport materials for OLEDs as well.

Keywords Diketopyrrolopyrrole derivatives · Chemosensor · Basis set superposition error (BSSE) correction · Atoms in molecules (AIM) · Natural bond orbitals (NBO)

Electronic supplementary material The online version of this article (doi:10.1007/s00214-012-1260-5) contains supplementary material, which is available to authorized users.

R. Jin (✉)
College of Chemistry and Chemical Engineering, Chifeng University, Chifeng 024000, China
e-mail: Ruifajin@163.com

1 Introduction

In the field of supramolecular chemistry, recognizing and sensing of anionic analytes has recently received significant attention because anions play an important role in a wide range of biological, environmental, and chemical processes [1–7]. Especially, fluorescent chemosensors that show the shift of emission bands upon binding to anions appear to be particularly attractive due to its simplicity, high sensitivity, and high selectivity [8, 9]. They provide immediate qualitative signal, which allows direct naked-eye detection of anions because of a specific color change of solution upon anion complexation [10–12]. The smallest anion, F^-, has unique chemical properties. It is of particular interest to detect it owing its essential roles in a broad range of biological, medical, and chemical processes of osteoporosis, fluorination of drinking water supplies, or even in chemical and nuclear warfare agents [13–15]. Therefore, noble methods for the detection of fluoride have become a hot topic. However, the chemosensors for F^- are rather few, and there is a need for good anion sensors with an improved specific response, in particular, in selectivity for F^- in the presence of Cl^- and Br^-. Furthermore, it is necessary to understand the unique host–guest interaction of the sensor with F^- from other halides anions. Different signaling mechanisms have been suggested for F^-, such as photoinduced electron transfer (PET) [16], excited state proton transfer (ESPT) [17], intramolecular charge transfer (ICT) [18, 19], excimer and exciplex formation [20], and metal–ligand charge transfer (MLCT) [21].

In parallel to recent experimental work on the chemosensors for F^-, theoretical efforts have indeed begun to constitute an important source of valuable information, complementing the experimental studies in the host–guest interaction and signaling properties. A number of studies

demonstrate the interplay between theory and experiment, which is capable of providing useful insights into the understanding of the molecular electronic structure of the ground and excited states as well as the nature of optical property for chemosensors [22–25].

1,4-Diketo-3,6-diphenylpyrrolo[3,4-c]pyrrole (DPP) and its derivatives represent a class of brilliant red and strongly fluorescent high-performance pigments because of their exceptional light, weather, and heat stability [26, 27]. Some DPP derivatives show good optical and electrical properties due to their high photoluminescence efficiency and good chemical and thermal stability [28, 29]. Furthermore, substances containing DPP fragment are promising materials for the constructing of organic light-emitting diodes (OLEDs) [30], polymer solar cells (PSCs) [31–33], two-photon absorption [34, 35], and field effect transistors (FET) [36]. Recently, a ratiometric fluorescent fluoride chemosensor as well as chromogenic chemosensor made of diketopyrrolopyrrole (DPP) derivatives has been reported [37]. F^--induced color change allows its detection with naked eyes. The changes in the electronic absorption and fluorescence behavior of DPP derivatives are due to F^--induced deprotonations of the active N-H group of diketopyrrolopyrrole moiety.

Herein, we report the investigation of both host–guest interaction and signaling properties from theoretical point of view for this system. Further in-depth interpretations of the available experimental electronic and spectroscopic characteristics have been discussed by the investigation of the optical and electronic properties of DPP derivatives. Furthermore, quantum chemical studies of the substitution effect on the electronic and optical properties of DPP derivatives are thereby called for designing novel functional materials. To investigate the substituent effect, several DPP derivatives (**1–7**), as shown in Scheme 1, have been designed by introducing functional groups on DPP. The optical and electronic properties of these derivatives are predicted to provide a demonstration for the rational design of new fluorescent and/or chromogenic chemosensors for fluoride anion, as well as some candidates for luminescent and charge transport materials for OLEDs.

2 Computational details

All calculations were performed using Gaussian 09 code [38]. Optimizations were carried out without symmetry constraints. On the basis of our previous successful calculation for some fluoride chemosensors [39–42], the geometries of **1–7** and their anions in ground states (S_0) were optimized by using the hybrid B3LYP functional with 6-31+G(d,p) basis set. Furthermore, complexes consisting of **1–7** and X^- (X = F, Cl, and Br) were optimized at the same theoretical levels as above with the consideration of the basis set superposition error (BSSE) correction using the counterpoise method [43]. The first excited singlet-state (S_1) structures for **1–7** and their anions were optimized at the TD-B3LYP level using 6-31+G(d,p) basis set. The harmonic vibrational frequency calculations using the same methods as for the geometry optimizations were used to ascertain the presence of a local minimum and to evaluate the zero-point energy corrections. Absorption and fluorescent properties of **1–7** and their anions were predicted using the TD-PBE0/6-31+G(d,p) method based on the S_0 and S_1 optimized geometries, respectively. To investigate the influence of solvents on the optical properties of the S_0 and S_1 states for the molecular systems in dichloromethane (DCM, dielectric constant: 8.93) solvent, we performed the polarized continuum model (PCM) [44] calculations at the TD-DFT level.

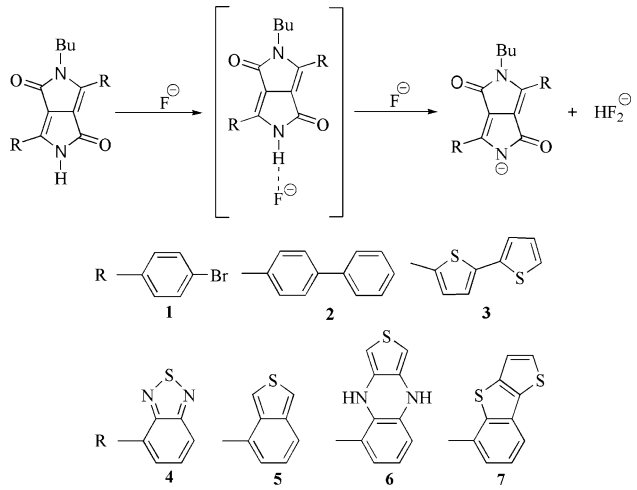

Scheme 1 Geometries of diketopyrrolopyrrole derivatives (**1–7**) and their deprotonation chemosensing processes for F^-. *Dotted lines* denote hydrogen bonds

To gain additional insight into the bonding characteristics of the studied complexes consisting of **1–7** and X^- (X = F, Cl, and Br), we used the atoms in molecules (AIM) [45, 46] theory at the B3LYP/6-31+G(d,p) level. The charge distribution was performed using the natural bond orbital (NBO) approach, which has been proven to be very valuable in the study and characterization of hydrogen bonds and cooperative effects [47].

The charge transfer rate can be described by Marcus theory [48, 49] via the following equation:

$$K = \left(V^2/\hbar\right)(\pi/\lambda k_B T)^{1/2}\exp(-\lambda/4k_B T) \quad (1)$$

where T is the temperature, k_B is the Boltzmann constant, λ represents the reorganization energy due to geometric relaxation accompanying charge transfer, and V is the electronic coupling matrix element (transfer integral) between the two adjacent species dictated largely by orbital

overlap. There are two major parameters that determine the self-exchange electron transfer rate: the V and λ. In order to investigate V (the charge transfer coupling integral for the electron/hole), crystal data in general are required [50–52]. However, the crystal data of our designed molecules are unavailable, and we cannot predict them due to the lack of available approaches. Thus, we focus on their reorganization energies λ to investigate their charge transport properties. Generally, the λ can be divided into two parts, external reorganization energy (λ_{ext}) and internal reorganization energy (λ_{int}). λ_{ext} represents the effect of polarized medium on charge transfer; on the other hand, λ_{int} is a measure of structural change between ionic and neutral states [53, 54]. Our designed molecules are used as charge transport materials for OLEDs in the solid film; the dielectric constant of the medium for the molecules is low. The computed values of the external reorganization energy in pure organic condensed phases are not only small but also much smaller than their internal counterparts [55–59]. Moreover, there is a clear correlation between λ_{int} and charge transfer rate in the literature [60, 61]. The reorganization energy could be an important factor that governs the mobility of charge carriers [62]. Therefore, we only pay attention to the discussion of the λ_{int} of the isolated active organic systems due to ignoring any environmental relaxation and changes in this paper. Our calculations of the reorganization energy associated with different geometries of two states are based on the hopping model schematically illustrated in Fig. 1. Moreover, in order to compare with the interested results reported previously [63–65], the reorganization energies for electron (λ_e) and hole (λ_h) of the molecules were predicted from the optimized neutral, cationic, and anionic geometries at the B3LYP/6-31G(d,p) level.

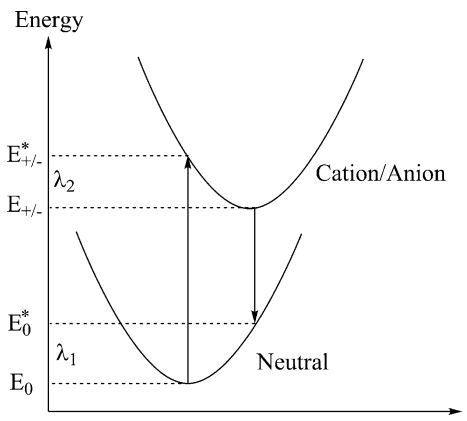

Fig. 1 Sketch of the potential energies of neutral and cation/anion species, illustrating the neutral (λ_1) and cation/anion (λ_2) relaxation energies

3 Results and discussion

3.1 Host–guest interaction

In order to obtain insight into the anion-sensing mechanism, the interactions between hosts and guests have been investigated exploiting the density functional method. Table 1 presents the most important geometrical parameters for complexes $\mathbf{1}^-\cdot$HF and $\mathbf{1}\cdot X^-$ (X = Cl and Br) with and without BSSE corrections. The geometries of the complexes $\mathbf{1}^-\cdot$HF and $\mathbf{1}\cdot X^-$ (X = Cl and Br) with BSSE corrections are shown in Fig. 2. The Cartesian coordinates of **1–7** along with their energies for the S_0 are given in Supplementary Table SI. The corresponding Cartesian coordinates of complexes for **1–7** along with their free energies for the S_0 are given in Supplementary Table SII. According to the suggested geometry cutoffs for D–H···A hydrogen bond definition, that is, H···A distances <3.0 Å and D–H···A angles >110° [66, 67], the interaction between pyrrole-N and H in complex $\mathbf{1}^-\cdot$HF and between Cl and Br and pyrrole-NH in $\mathbf{1}\cdot X^-$ (X = Cl and Br) can be identified as hydrogen bonds. Comparing the optimized geometries with and without BSSE corrections, one may find that the deviations of the hydrogen bond length between pyrrole-N and H ($R_{N\cdots H}$) and the distance between H and F (R_{H-F}) in complex $\mathbf{1}^-\cdot$HF are 0.008 and 0.002 Å, respectively. The corresponding deviation of the angles $\theta_{N-H\cdots F}$ in complex $\mathbf{1}^-\cdot$HF is 0.1°. Therefore, BSSE correction is necessary for the optimization of this kind of system to some extent. Compared with the H–N bond in **1** (1.009 Å), obviously, the H–N bond is broken (0.487 Å elongation) and $R_{H\cdots N} = 1.496$ Å and $R_{H-F} = 1.018$ Å forming $\mathbf{1}^-\cdot$HF. For chemosensors **n** (n = 2–7), the values of $R_{H\cdots N}$ in complexes $\mathbf{n}^-\cdot$HF (n = 2–7) are 1.502, 1.492, 1.527, 1.509, 1.627, and 1.494 Å, while the corresponding values of R_{H-N} in neutral chemosensors **n** (n = 2–7) are all 1.009 Å as in **1** (see Tables SI and SII in Supplementary). It suggests that the H–N bonds are broken (0.485–0.618 Å elongation) forming $\mathbf{n}^-\cdot$HF. Namely, the pyrrole-NH moieties of chemosensors **n** (n = 1–7) can be efficiently deprotonated by F^-. In the cases of Cl^- and Br^-, however, R_{H-N} values only change slightly (<0.05 and 0.04 Å elongations, respectively). It suggests that deprotonations indeed take place from the acidic pyrrole-NH of host chemosensors to form $\mathbf{n}^-$ and HF in the presence of F^-. However, for Cl^- and Br^-, the host chemosensors prefer to form the hydrogen-bonded complexes between **n** and Cl^- and Br^-, rather than formation of $\mathbf{n}^-$ forms. Comparing the signaling properties of chemosensors **1–7** for F^- with other chemosensors in our previous works, one can find that the F^- detecting properties of **1–7** are similar to those of 2-(2-hydroxyphenyl)-1,3,4-oxadiazole and coumarin derivatives [39, 40]. However, the signaling properties of chemosensors

Table 1 The distances of R_{N-H} and $R_{H\cdots X}$ (in angstroms) and H-bond angles of $\theta_{N-H\cdots X}$ (in deg) in complexes $\mathbf{1}^-\cdot$HF and $\mathbf{1}\cdot X^-$ (X = Cl and Br) with and without BSSE corrections at the B3LYP/6-31+G(d,p) level

Species	Without BSSE			With BSSE		
	R_{N-H}	$R_{H\cdots X}$	$\theta_{N-H\cdots X}$	R_{N-H}	$R_{H\cdots X}$	$\theta_{N-H\cdots X}$
1	1.009					
$\mathbf{1}^-\cdot$HF	1.496	1.018	175.5	1.504	1.016	175.4
$\mathbf{1}\cdot Cl^-$	1.057	2.061	178.2	1.056	2.065	178.2
$\mathbf{1}\cdot Br^-$	1.051	2.193	179.0	1.046	2.299	179.2

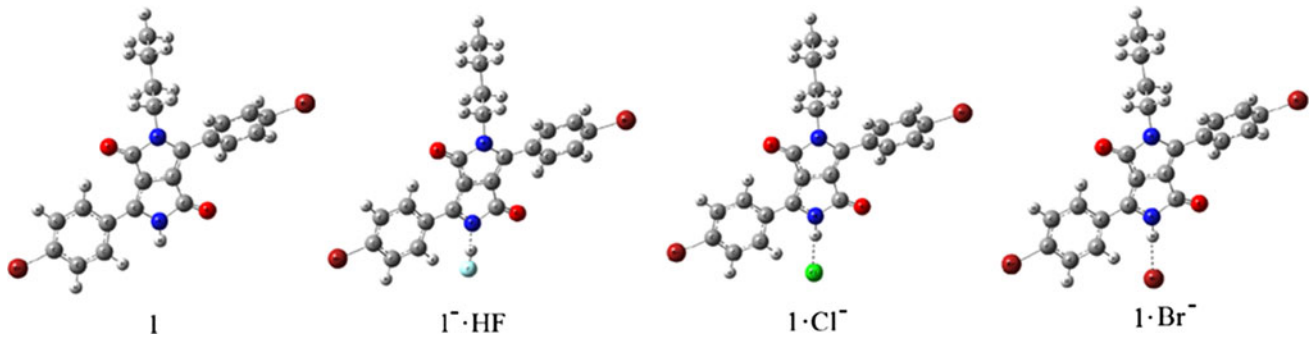

Fig. 2 Geometries of the complexes $\mathbf{1}^-\cdot$HF and $\mathbf{1}\cdot X^-$ (X = Cl and Br) with BSSE corrections at the B3LYP/6-31+G(d,p) level

Table 2 The ΔG_{BSSE} ($G_{BSSE} = G(\mathbf{n}\cdot X^-) - [G(\mathbf{n}) + G(X^-)]$, in kcal/mol) of complexes $\mathbf{n}^-\cdot$HF, $\mathbf{n}\cdot Cl^-$, and $\mathbf{n}\cdot Br^-$ (n = 1–7) at the B3LYP/6-31+G(d,p) level

n	$\mathbf{n}^-\cdot$HF	$\mathbf{n}\cdot Cl^-$	$\mathbf{n}\cdot Br^-$
1	−52.3	−20.2	−21.8
2	−47.8	−16.8	−17.9
3	−50.1	−18.5	−19.5
4	−56.8	−22.6	−23.8
5	−47.8	−15.9	−17.3
6	−53.2	−19.5	−20.5
7	−49.7	−18.1	−19.8

1–7 for F^- are different from the chemosensors of both thiazole and aminophthalimide derivatives, which prefer to bind with F^- and form the complexes, rather than formation of anion forms [41, 42]. Different chemosensors for F^- show that different detecting properties may be attributed to the geometry of the active moieties for F^-, which should be taken into account for the future studies.

The BSSE-corrected interaction free energies (ΔG_{BSSE}, in which the vibrational contributions include zero-point vibrational energy) of $\mathbf{n}^-\cdot$HF and $\mathbf{n}\cdot X^-$ (n = 1–7, X = Cl and Br) are calculated based on of the optimized geometries with BSSE correction. The ΔG_{BSSE} values of $\mathbf{n}^-\cdot$HF and $\mathbf{n}\cdot X^-$ (n = 1–7, X = Cl and Br) are listed in Table 2. It is clear that the ΔG_{BSSE} of complexes $\mathbf{n}^-\cdot$HF (n = 1–7) are much more favorable for the distinct selectivity of F^- than other halide anions. Furthermore, complexes $\mathbf{n}\cdot X^-$ (n = 1–7, X = Cl and Br) are only hydrogen-bonded complexes in nature. The deprotonations do not take place from the acidic pyrrole-NH of host chemosensors to form anions as in the presence of F^-. It indicates that the absorption and fluorescent properties of the host chemosensors are similar to those before the addition of Cl^- or Br^-. These calculation results are in good agreement with the reported experimental observations that intermolecular proton transfer (IPT) between chemosensor substrate **1** and F^- occurs when the concentration of F^- reaches certain level from the addition of F^- to the chemosensor solution [37]. Inspection of Table 2 reveals clearly that the ΔG_{BSSE} values of complexes $\mathbf{n}^-\cdot$HF (n = 2–7) are similar to that of $\mathbf{1}^-\cdot$HF (the deviations are within 4.5 kcal/mol). This indicates that the different functional group substituents do not significantly affect the ΔG_{BSSE} values compared with that of **1**. However, the ΔG_{BSSE} values of complexes $\mathbf{n}^-\cdot$HF (n = 1–7) are more than twice as those of $\mathbf{n}\cdot X^-$ (n = 1–7, X = Cl and Br), respectively. Thus, one can conclude that the host chemosensors have much stronger affinity to F^- than to Cl^- and Br^- through intermolecular proton transfer, which leads to the formation of chemosensors anions by F^-. The hydrogen bond acceptor F^- is stronger than those of Cl^- and Br^-, respectively. On the other hand, the more pronounced the proton transfer reaction, the higher the

intensity of the hydrogen bond interaction and the higher the stability of the complex [67, 68]. Furthermore, the ΔG_{BSSE}, R_{H-N}, and R_{H-X} (X = F, Cl, and Br) values of complexes also support the distinct selectivity for F^- from Cl^- and Br^-.

3.2 AIM and NBO analysis

The AIM theory is often applied to study hydrogen bonds [69–71]. The characteristics of bond critical points (BCPs) are very useful to estimate the strength of hydrogen bonds. To gain a deeper insight into the fundamental nature of NH···X (X = F, Cl, and Br) hydrogen bonds, it is crucial to obtain reasonable estimates of their relative energies. In particular, the electron densities, $\rho(r)_{bcp}$, and their Laplacians, $\nabla^2\rho(r)_{bcp}$, evaluated at BCPs are frequently used as indicators of hydrogen bond. More specifically, the kinetic $G(r)_{bcp}$ and potential $V(r)_{bcp}$ electron energy densities are often used to gain additional insight into the strength and nature of a given hydrogen bond. The local kinetic electron energy density can be evaluated from the values of $\rho(r)_{bcp}$ and $\nabla^2\rho(r)_{bcp}$ as [72]

$$G(r)_{bcp} = \frac{3}{10}(3\pi)^{2/3}\rho(r)_{bcp}^{5/3} + \frac{1}{6}\nabla^2\rho(r)_{bcp} \quad (2)$$

The kinetic energy density $G(r)_{bcp}$ is in turn related to the potential energy density $V(r)_{bcp}$ through the local statement of the virial theorem [73]:

$$V(r)_{bcp} = \frac{\hbar^2}{4m}\nabla^2\rho(r)_{bcp} - 2G(r)_{bcp}. \quad (3)$$

The hydrogen bond energy E_{HB} (defined as $-D_e$, where D_e is the hydrogen bond dissociation energy) in molecules can be estimated within the framework of the AIM analysis using the relationship [74]:

$$E_{HB} = -D_e = 0.5V(r)_{bcp} \quad (4)$$

The $\rho(r)_{bcp}$, $\nabla^2\rho(r)_{bcp}$, and E_{HB} of the complexes $\mathbf{n}^-$·HF and $\mathbf{n}$·X^- (n = 1–7, X = Cl and Br) are given in supplementary Tables SIII and SIV, respectively. As a general rule, hydrogen bonds are characterized by positive values of $\nabla^2\rho(r)_{bcp}$ and low $\rho(r)_{bcp}$ values (<0.1). Covalent bonds (shared interactions) have negative $\nabla^2\rho(r)_{bcp}$ values and high values of $\rho(r)_{bcp}$, whereas the values of $\nabla^2\rho(r)_{bcp}$ become positive when the bonds contain the ionic nature [75]. The results displayed in Table SIII reveal that the $\rho(r)_{bcp}$ and $\nabla^2\rho(r)_{bcp}$ values of H···N in $\mathbf{n}^-$·HF (n = 1–7) are about 0.08 and 0.07, respectively. It suggests that the interactions between N and H in $\mathbf{n}^-$·HF (n = 1–7) are hydrogen bonds in nature. The $\rho(r)_{bcp}$ and $\nabla^2\rho(r)_{bcp}$ values of H–F in $\mathbf{n}^-$·HF (n = 1–7) are about 0.26 and −1.20, respectively. Hence, H–F bonds of $\mathbf{n}^-$·HF (n = 1–7) contain the covalent bond nature. On the contrary, for complexes $\mathbf{n}$·X^- (n = 1–7, X = Cl and Br), BCPs at H–N provides $\nabla^2\rho(r)_{bcp} < 0$ (about −1.5) and high positive values for $\rho(r)_{bcp}$ (about 0.3), which are characteristics of covalent type interactions. For H···X bonds in complexes $\mathbf{n}$·X^- (n = 1–7, X = Cl and Br), the values of $\rho(r)_{bcp}$ and $\nabla^2\rho(r)_{bcp}$ are about 0.03 and 0.06, respectively. It indicates that H···X bonds in complexes $\mathbf{n}$·X^- (n = 1–7, X = Cl and Br) show hydrogen bond characteristics. Furthermore, the E_{HB} values of H···N and H···X in complexes confirm the expectation. The E_{HB} values of H···N bonds in $\mathbf{n}^-$·HF (n = 1–7) are more negative than those of H···X bonds in $\mathbf{n}$·X^- (n = 1–7, X = Cl and Br), indicating that the strength of H···N hydrogen bonds in $\mathbf{n}^-$·HF (n = 1–7) is stronger than that of H···X hydrogen bonds in $\mathbf{n}$·X^- (n = 1–7, X = Cl and Br). The above results show qualitative agreement with the results based on their geometries.

It is well known that the electronic reorganization derived from the formation of a hydrogen bond is associated with a charge transfer between the two moieties of the complex [66]. The overall NBO charge transfer has been evaluated by summing up the NBO atomic charges on the two moieties of each hydrogen-bonded complex (the host chemosensors and halides). We select the parent compound **1** as representative of the system under investigation. The calculated NBO charge densities for $\mathbf{1}^-$·HF and **1**·X^- (X = Cl and Br) are collected in supplementary Table SV. It clearly shows that the sum of the charges on the $\mathbf{1}^-$ moiety is −0.876, while the corresponding value of HF is only −0.124 in complex $\mathbf{1}^-$·HF. The sum of charges on the **1** moiety and Cl^- in **1**·Cl^- are −0.160 and −0.840, while the corresponding values in **1**·Br^- are −0.145 and −0.855, respectively. Hence, the NBO charge analysis also indicates that the proton is almost completely abstracted by F^-. In the cases of Cl^- and Br^-, however, the host chemosensor prefers to form the hydrogen-bonded complexes between **1** and Cl^- and Br^-, rather than formation of $\mathbf{1}^-$ form.

3.3 Electronic transition

It is well known that the frontier molecular orbitals (FMOs) and HOMO–LUMO gaps (E_g) values are heavily related to the optical and electronic properties. An electronic excitation results in some electron density redistribution that affects the molecular geometry [76]. To gain insight into the influence of the optical and electronic properties, the distributions of the FMOs in S_0 for **1** and $\mathbf{1}^-$ are investigated, and their sketches are plotted in Fig. 3. The major assignments of the lowest electronic transitions for **1** and $\mathbf{1}^-$ are mainly as HOMO → LUMO, which corresponds to a $\pi - \pi^*$ excited singlet state as visualized in Fig. 3. For **1**, the HOMO and LUMO are spread over the whole conjugated molecule. However, the HOMO of $\mathbf{1}^-$ is mainly

localized on diketopyrrolopyrrole and 8-bromobenzene moieties, while its LUMO is spread over the whole conjugated molecule. These results reveal that the F^- has obvious effect on the distribution of FMOs. This implies that the deprotonation influences the distributions of FMOs for host chemosensor.

Another way to understand the influence of the optical and electronic properties is to analyze the E_{HOMO}, E_{LUMO}, and E_g values. We calculated the FMO energies of **1** and $\mathbf{1}^-$ (see Fig. 4) in both S_0 and S_1 at the B3LYP/6-31+G(d,p) and TD-B3LYP/6-31+G(d,p) levels, respectively. Both the E_{HOMO} and E_{LUMO} values of $\mathbf{1}^-$ in S_0 are higher than those of **1**, respectively. However, the prediction of E_g value of $\mathbf{1}^-$ is lower than that of **1**. This shows that $\mathbf{1}^-$ possesses higher values of both E_{LUMO} and E_{HOMO} and smaller value of E_g in comparison with **1**. These results suggest that the deprotonation can reduce the E_g value of host chemosensor. This can be explained by the fact that the $\mathbf{1}^-$ has better conjugation due to small twist angles between diketopyrrolopyrrole and 8-bromobenzene. The dihedral values of between diketopyrrolopyrrole and 8-bromobenzene for **1** and $\mathbf{1}^-$ are 37.9 and 20.5°, respectively. It suggests that the molecular p-conjugation in $\mathbf{1}^-$ becomes higher than that in **1**. Similar phenomena are also found for S_1. These results reveal that the deprotonation by F^- has obvious effect on the distribution of FMOs, resulting in the large redshift between their UV–vis spectra.

3.4 Optical properties

The original color and emissions of chemosensors change upon addition of F^- because of formation anions. The Cartesian coordinates of **1–7** anions along with their energies for the S_0 are given in Supplementary Table SVI. The corresponding Cartesian coordinates of **1–7** and their anions along with their energies for the S_1 are given in Supplementary Tables SVII and SVIII, respectively. The bathochromic or hypsochromic shifts between the two characteristic absorption and emissions of **1** and $\mathbf{1}^-$ are chosen to calculate the colorimetric and fluorescent fluoride anion chemosensor, respectively. Table 3 presents the absorption λ_{abs} and fluorescence λ_{fl} wavelengths, assignments, and the oscillator strength f for **1** with and without F^- in DCM at the TD-PBE0/6-31+G(d,p) level. The λ_{abs} and λ_{fl} values are all in agreement with the experimental results [37]. Namely, $\lambda_{abs} = 477$ and 571 nm and

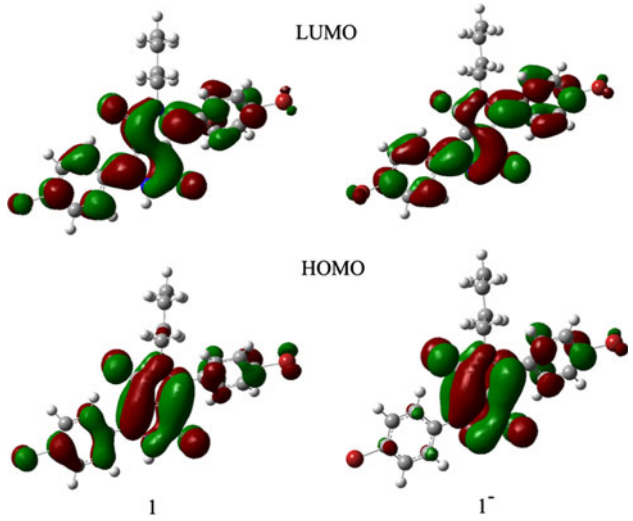

Fig. 3 FMOs of **1** and $\mathbf{1}^-$ in S_0 at the B3LYP/6-31G+(d,p) level

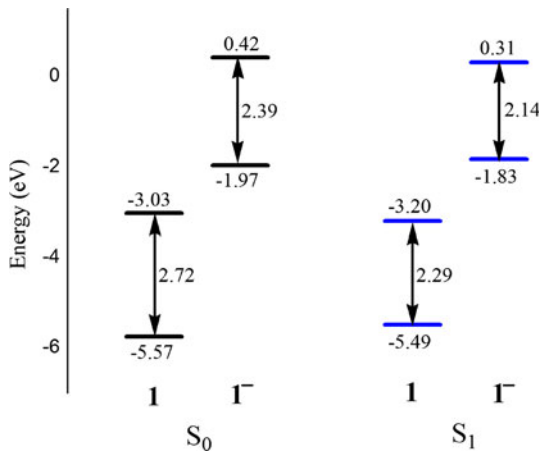

Fig. 4 Evaluation of calculated FMOs energies in S_0 and S_1 for **1** and $\mathbf{1}^-$ at the B3LYP/6-31+G(d,p) and TD-B3LYP/6-31+G(d,p) levels, respectively

Table 3 The absorption (λ_{abs}) and fluorescence (λ_{fl}) wavelengths (in nm), oscillator strength f, and assignments (coefficient) for **1** with and without F^- in DCM at the TD-PBE0/6-31+G(d,p) level, along with available experimental data

Conditions	Absorption				Fluorescence			
	λ_{abs}	f	Assignments	Exp[a]	λ_{fl}	f	Assignments	Exp[a]
Without F^-	483	0.69	H → L (0.71)	477	566	0.74	H ← L (0.71)	531
With F^-	544	0.46	H → L (0.70)	571	613	0.44	H ← L (0.70)	613

[a] Experimental results were taken from Ref. [37]

Table 4 The absorption (λ_{abs}) wavelengths (in nm), oscillator strength *f*, and assignments (coefficient) for **n** and $\mathbf{n}^-$ ($n = 1$–7) in DCM at the TD-PBE0/6-31+G(d,p) level, along with available experimental data

n	**n**				$\mathbf{n}^-$			
	λ_{abs}	*f*	Assignment	Exp[a]	λ_{abs}	*f*	Assignment	Exp[a]
1	483	0.69	H → L (0.71)	477	544	0.46	H → L (0.70)	571
2	498	0.97	H → L (0.71)	485	565	0.66	H → L (0.70)	585
3	616	1.39	H → L (0.71)		661	0.99	H → L (0.71)	
4	550	0.57	H → L (0.71)		712	0.38	H → L (0.70)	
5	531	0.72	H → L (0.71)		598	0.49	H → L (0.70)	
6	648	0.56	H → L (0.71)		905	0.36	H → L (0.70)	
7	521	1.28	H → L (0.71)		579	0.81	H → L (0.70)	

[a] Experimental results were taken from Ref. [37]

$\lambda_{fl} = 531$ and 613 nm before and after the addition of F^-, respectively. The bathochromic shifts between the two characteristic λ_{abs} and λ_{fl} values for **1** and $\mathbf{1}^-$ are 61 and 47 nm, which are comparable to the experimental values of 94 and 82 nm, respectively. Thus, these results credit to the computational approach, so appropriate electronic transition energies can be predicted at these levels for such kind of chemosensor. The successful simulations indicate that the observed colorimetric and fluorescent signals truly originate from the formation of $\mathbf{1}^-$ anion.

In general, the sensing procedures and spectral parameters of chemosensors can also been affected by solute–solvent-specific interactions like hydrogen bonding [77, 78]. Therefore, we select highly H-bonded solvent water to estimate the effect of solvent on the sensing procedures and on the spectral parameters of the chemosensor **1**. The results suggest that the water effects do not significantly affect the deprotonation process of chemosensor by F^-. Furthermore, the absorption and fluorescence spectra of **n** ($n = 1$–7) in DCM are similar to those in water (see detail discussion and Fig. SI and Tables SIX and SX in Supplementary).

Table 4 presents the absorption wavelengths λ_{abs} and the oscillator strength (*f*) of **1**–**7** and their anions in DCM. The λ_{abs} of **2**, **5**, and **7** have slight bathochromic shifts, the deviations are within 48 nm, whereas **3**, **4**, and **6** have strong bathochromic shifts compared with that of the parent chemosensor **1**, the deviations being 67, 133, and 165 nm, respectively. In general, larger oscillator strength corresponds to larger experimental absorption coefficient or stronger fluorescence intensity. The *f* values of **2**–**7** are similar to that of **1** except that the *f* values of **3** and **7** are larger than that of **1**. It suggests that all derivatives correspond to more intensive spectrum. For the $\mathbf{n}^-$ of the substituted derivatives, it is found that the λ_{abs} of $\mathbf{2}^-$, $\mathbf{5}^-$, and $\mathbf{7}^-$ have slight bathochromic shifts, the deviations are within 54 nm, while the corresponding values of $\mathbf{3}^-$, $\mathbf{4}^-$, and $\mathbf{6}^-$ have strong bathochromic shifts compared with that of $\mathbf{1}^-$. The *f* values of $\mathbf{2}^-$, $\mathbf{3}^-$, **5**, and $\mathbf{7}^-$ are larger than that of $\mathbf{1}^-$, while the corresponding values of **4** and **6** are slightly less than that of **1**. It clearly shows that the functional groups in **3**, **4**, and **6** have more influence on the shifts of λ_{abs} for the substituted derivatives and their anions, while the functional groups in **2**, **5**, and **7** do not significantly affect the λ_{abs} of the substituted derivatives and their anions. Furthermore, derivatives **3** and **7** and their anions show the most intensive spectrum among the substituted derivatives and their anions.

On the basis of the results displayed in Table 4 and taking into account the ΔG_{BSSE}, one can conclude that all the substituted derivatives **2**–**7** are expected to be chromogenic chemosensors. The bathochromic shifts between the two characteristic λ_{abs} values of **n** and $\mathbf{n}^-$ ($n = 2$–7, i.e., λ_{abs} values before and after the addition of F^-) are 67, 45, 162, 67, 257, and 58 nm, respectively. Therefore, the orange red solution of **2** turns purple red in the present F^- as observed in experiment [37]. The red solutions of **5** and **7** turn blue and purple, while the blue green, purple red, and green solutions of **3**, **4**, and **6** turn red, yellow green, and colorless upon addition of F^-, respectively.

Table 5 lists the fluorescence wavelengths λ_{fl} and the oscillator strength (*f*) of **1**–**7** and their anions in DCM. The λ_{fl} values of **2**–**7** and their anions have bathochromic shifts compared with those of the parent compound **1** and its anion $\mathbf{1}^-$, respectively. Hence, all substituents can significantly affect the fluorescence spectra of the substituted derivative **2**–**7** and their anions. Furthermore, the *f* values of **4**–**6** and their anions are similar to those of **1** and $\mathbf{1}^-$, whereas the corresponding values of **2**, **3**, and **7** and their anions are larger than those of **1** and $\mathbf{1}^-$, respectively. It indicates that **2**, **3**, and **7** and their anions correspond to strong fluorescence spectra. Thus, one may conclude that the fluorescence intensity can be increased by introduction of the functional groups on the parent chemosensor **1**. This indicates that the substituted derivatives **1**–**7** are promising luminescent materials for OLEDs as well, particularly for **2**, **3**, and **7**.

Table 5 The fluorescence (λ_{fl}) wavelengths (in nm), oscillator strength f, and assignments (coefficient) for **n** and $\mathbf{n}^-$ (n = 1–7) in DCM at the TD-PBE0/6-31+G(d,p) level, along with available experimental data

n	**n**				$\mathbf{n}^-$			
	λ_{fl}	f	Assignment	Exp[a]	λ_{fl}	f	Assignment	Exp[a]
1	566	0.74	H ← L (0.71)	531	613	0.44	H ← L (0.70)	613
2	592	1.11	H ← L (0.71)	545	645	0.69	H ← L (0.71)	630
3	698	1.44	H ← L (0.71)		746	0.98	H ← L (0.71)	
4	634	0.61	H ← L (0.71)		857	0.21	H ← L (0.70)	
5	604	0.83	H ← L (0.71)		684	0.41	H ← L (0.71)	
6	741	0.58	H ← L (0.71)		856	0.23	H ← L + 1 (0.71)	
7	609	1.36	H ← L (0.71)		650	0.81	H ← L (0.71)	

[a] Experimental results were taken from Ref. [37]

The results displayed in Table 5 and considering the ΔG_{BSSE} values indicate that all the substituted derivatives **n** (n = 2–7) are expected to be promising candidates for ratiometric fluorescent fluoride chemosensors. The bathochromic shifts between the two characteristic λ_{fl} values of **n** and $\mathbf{n}^-$ (i.e., λ_{fl} values before and after the addition of F^-) are 53, 48, 223, 80, 115, and 41 nm, respectively. Therefore, the yellow, red, amber, and orange original emissions of **2**, **3**, **5**, and **7** may be quenched, and new carmine, cherry, red, and cardinal red emissions appear upon the addition of F^-, respectively. However, the orange red and cherry original emissions of **4** and **6** turn colorless in the present F^-.

3.5 Charge transfer and stability properties

The calculated absolute hardness and reorganization energies for hole and electron are listed in Table 6. It is well known that the lower the reorganization energy values, the higher the charge transfer rate [48, 49]. The reorganization energy refers to the whole system formed by donor, acceptor, and media. The environment (usually a solvent) plays a major role in the reorganization energy, since the charge species are generally stabilized in a very different way by the solvent. To evaluate the impact of solvent effects on the reorganization energy of **1**–**7**, we have selected benzene, ether, and tetrahydrofuran (their dielectric constants are 2.247, 4.335, and 7.58, respectively) as representatives. The calculated results are shown in supplementary Table SXI. These results reveal that different solvents (both polar and nonpolar) at PCM level used in this study have slight effects on the λ_e and λ_h values of **1**–**7**. Thus, the solvent effect for investigated system is negligible in this work. The results displayed in Table 6 show that the calculated λ_e values of the substituted derivatives (0.177–0.269 eV) are much smaller than that of tris(8-hydroxyquinolinato)aluminum(III) (Alq3) (λ_e = 0.276 eV), a typical electron transport material [65]. It indicates that their electron transfer rates may higher than that of Alq3. From Table 6, one can find that the smallest λ_e values in these derivatives are found in **3** and **6** (λ_e = 0.164 and 0.177 eV), suggesting that **3** and **6** could be good electron transfer materials from the standpoint of the λ_e values. On the other hand, the λ_h values of **1**–**4** and **7** (0.272–0.362 eV) are larger than that of *N*,*N*′-diphenyl-*N*,*N*′-bis(3-methlphenyl)-(1,1′-biphenyl)-4,4′-diamine (TPD), which is a typical hole transport material (λ_h = 0.290 eV) [63]. The λ_h values of **5** and **6** are slightly smaller than that of TPD. It implies that the hole transfer rates of **1**–**7** might be lower than that of TPD. Inspection of Table 6 reveals clearly that the largest reorganization energy in these derivatives is found in **1** (λ_h = 0.362 eV, λ_e = 0.266 eV) except for λ_e value of **2**, suggesting that the substitution may decrease the λ_h and λ_e. However, the λ_h values of substituted derivatives are larger than that of TPD, while the λ_e values of substituted derivatives are much smaller than that of Alq3. It indicates that **1**–**7** can be used as promising electron transport materials in the organic light-emitting diodes (OLEDs) from the standpoint of the smaller reorganization energy.

Table 6 The calculated λ_e, λ_h, and η (all in eV) of **1**–**7** at the B3LYP/6-31G(d,p) level

Compounds	λ_h	λ_e	η
1	0.362	0.266	2.504
2	0.346	0.269	2.352
3	0.295	0.164	2.080
4	0.325	0.257	2.299
5	0.272	0.254	2.306
6	0.273	0.177	1.995
7	0.329	0.235	2.252

As the stability is a useful criterion to evaluate the nature of devices for charge transport and luminescent

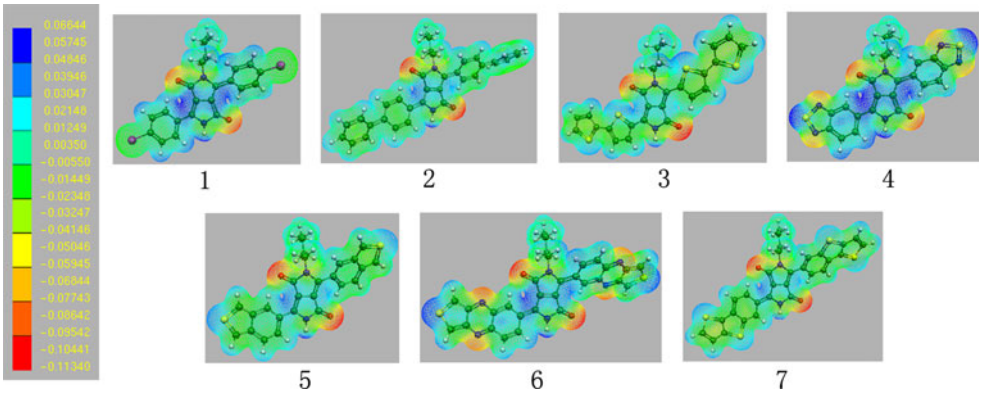

Fig. 5 Electrostatic surface potentials for **1–7** (regions of higher electron density are shown in *red* and of lower electron density in *blue*)

materials, to predict the stability of **1–7** from a viewpoint of molecular orbital theory, the absolute hardness, η, of **1–7** was calculated using operational definitions [79, 80] given by:

$$\eta = \frac{1}{2}\left(\frac{\partial \mu}{\partial N}\right) = \frac{1}{2}\left(\frac{\partial^2 E}{\partial N^2}\right) = \frac{\mathrm{IP} - \mathrm{EA}}{2} \tag{5}$$

where μ is the chemical potential and N is the total electron number. In this work, the values for IP (ionization potential) and EA (electron affinity) were determined according to the equation $\mathrm{IP} = E_{\mathrm{cr}} - E_{\mathrm{p}}$ and $\mathrm{EA} = E_{\mathrm{p}} - E_{\mathrm{ar}}$, where p, cr, and ar indicate the parent molecule and the corresponding cation and anion radical generated after electron transfer.

The absolute hardness η is the resistance of the chemical potential to change in the number of electrons. The results displayed in Table 6 reveal that the η values of **2–7** are similar to that of **1**, indicating that the stabilities of **2–7** are equal to that of **1**. Furthermore, the electrostatic surface potentials of investigated molecules were calculated as shown in Fig. 5. From Fig. 5, one can find that the partial positive charges are on the hydrogen atoms and/or sulfur atoms, while very large negative charges are on the oxygen atoms of diketopyrrolopyrrole rings and/or less negative charges on the nitrogen atoms for all **1–7**. These results reveal that the substitution effect does not significantly affect the stability of the substituted derivatives. The above results show qualitative agreement with the results based on the absolute hardness.

4 Conclusions

Our calculated results for both the host–guest interaction and the nature of colorimetric and fluorescent signaling for **1** in the presence of F^- are in good agreement with the reported experimental observations. The host chemosensor **1** has much stronger affinity to F^- than to Cl^- and Br^- through intermolecular proton transfer, which leads to the formation of chemosensor anion by F^-. The AIM theory and NBO charge analysis of the complexes consisting of **1** and X^- (X = F, Cl, and Br) confirm that the protons are almost completely abstracted by F^-. The FMO analysis has turned out that the deprotonation increases both E_{LUMO} and E_{HOMO} values and reduces the E_{g} values of host chemosensor in both S_0 and S_1. The study of substituent effects suggests that all the substituted derivatives are expected to be promising candidates for ratiometric fluorescent fluoride chemosensors as well as chromogenic chemosensors. Furthermore, the derivatives **2**, **3**, and **7** are promising luminescent materials, while derivatives **1–7** can serve as good electron transport materials for OLEDs, particularly for **3** and **6**.

Acknowledgments The author received financial supports from the Natural Science Foundation of Inner Mongolia Autonomous Region (No. 2011ZD02).

References

1. Bianchi A, Bowman-James K, Garcia-Espana E (1997) Supramolecular chemistry of anions. Wiley-VCH, New York
2. Deng Y, Chen Y, Cao D, Liu Z, Li G (2010) Sensors Actuat B Chem 149:165
3. Rhee HW, Choi SJ, Yoo SH, Jang YO, Park HH, Hun HP, Pinto RM, Cameselle JC, Sandoval FJ, Roje S, Han K, Chung DS, Suh J, Hong JI (2009) J Am Chem Soc 131:10107
4. Li JQ, Li XY (2007) J Phys Chem A 111:13061
5. Hagihara S, Tanaka H, Matile S (2008) J Am Chem Soc 130:5656
6. Yoon J, Kim SK, Singh NJ, Kim KS (2006) Chem Soc Rev 35:355
7. Gale PA (2006) Acc Chem Res 39:465
8. Callan JF, de Silva AP, Magri DC (2005) Tetrahedron 61:8551
9. Martinez-Manez R, Sancanon F (2003) Chem Rev 103:4419
10. Wu CY, Chen MS, Lin CA, Lin SC, Sun SS (2006) Chem Eur J 12:2263
11. Evans LS, Gale PA, Light ME, Quesada R (2006) Chem Commun 965
12. Coll C, Martínez-Máñez R, Dolores MM, Sancenón F, Soto J (2007) Angew Chem Int Ed 46:1675
13. Cametti M, Rissanen K (2009) Chem Commun 2809

14. Kirk KL (1991) Biochemistry of the halogens and inorganic halides. Plenum Press, New York
15. Zhang SW, Swager TM (2003) J Am Chem Soc 125:3420
16. Kim SK, Yoon J (2002) Chem Commun 770
17. Peng X, Wu Y, Fan J, Tian M, Han K (2005) J Org Chem 70:10524
18. Li Z, Zhang J (2006) Chem Phys 331:159
19. Thiagarajan V, Ramamurthy P (2007) J Lumin 126:886
20. Kim SK, Bok JH, Bartsch RA, Lee JY, Kim JS (2005) Org Lett 7:4839
21. Chow CF, Chiu BKW, Lam MHW, Wong WY (2003) J Am Chem Soc 125:7802
22. Yu F, Li P, Li G, Zhao G, Chu T, Han K (2011) J Am Chem Soc 133:11030
23. Li GY, Chu T (2011) Phys Chem Chem Phys 13:20766
24. Li G, Zhao G, Liu Y, Han K, He G (2010) J Comput Chem 31:1759
25. Li Z, Zhang J (2006) Chem Phys 331:159
26. Hao Z, Iqbal A (1997) Chem Soc Rev 26:203
27. Mizuguchi J, Giller G, Baeriswyl E (1994) J Appl Phys 75:514
28. Baheti A, Tyagi P, Thomas KRJ, Hsu YC, Lin JT (2009) J Phys Chem C 113:8541
29. Zhou EJ, Cong JZ, Yamakawa S, Wei QS, Nakamura M, Tajima K, Yang CH, Hashimoto K (2010) Macromolecules 43:2873
30. Zhu Y, Rabindranath AR, Beyerlein T, Tieke B (2007) Macromolecules 40:6981
31. Wienk MM, Turbiez M, Gilot J, Janssen RAJ (2008) Adv Mater 20:2556
32. Thompson BC, Fréchet JMJ (2008) Angew Chem Int Ed 47:58
33. Tamayo AB, Walker B, Nguyen TQ (2008) J Phys Chem C 112:11545
34. Jiang Y, Wang Y, Hua J, Qian S, Tian H (2009) J Polym Sci Part A 47:4400
35. Guo EQ, Ren PH, Zhang YL, Zhang HC, Yang WJ (2009) Chem Commun 5859
36. Yanagisawa H, Mizuguchi J, Aramakil S, Sakai Y (2008) Jpn J Appl Phys 47:4728
37. Qu Y, Hua J, Tian H (2010) Org Lett 12:3320
38. Frisch MJ, Trucks GW, Schlegel HB, Scuseria GE, Robb MA, Cheeseman JR, Scalmani G, Barone V, Mennucci B, Petersson GA, Nakatsuji H, Caricato M, Li X, Hratchian HP, Izmaylov AF, Bloino J, Zheng G, Sonnenberg JL, Hada M, Ehara M, Toyota K, Fukuda R, Hasegawa J, Ishida M, Nakajima T, Honda Y, Kitao O, Nakai H, Vreven T, Montgomery JA Jr, Peralta JE, Ogliaro F, Bearpark M, Heyd JJ, Brothers E, Kudin KN, Staroverov VN, Kobayashi R, Normand J, Raghavachari K, Rendell A, Burant JC, Iyengar SS, Tomasi J, Cossi M, Rega N, Millam JM, Klene M, Knox JE, Cross JB, Bakken V, Adamo C, Jaramillo J, Gomperts R, Stratmann RE, Yazyev O, Austin AJ, Cammi R, Pomelli C, Ochterski JW, Martin RL, Morokuma K, Zakrzewski VG, Voth GA, Salvador P, Dannenberg JJ, Dapprich S, Daniels AD, Farkas O, Foresman JB, Ortiz JV, Cioslowski J, Fox DJ (2009) Gaussian 09. Gaussian, Inc., Wallingford
39. Jin R, Ahmad Irfan A (2012) Comput Theor Chem 986:93
40. Jin R, Zhang J (2011) Chem Phys 380:17
41. Jin R (2011) J Fluorine Chem 132:907
42. Jin R, Zhang J (2009) Theor Chem Acc 124:225
43. Simon S, Duran M, Dannenberg JJ (1996) J Chem Phys 105:11024
44. Cornard JP, Lapouge C (2006) J Phys Chem A 110:7159
45. Bader RFW (1998) J Phys Chem A 102:7314
46. AIM2000 designed by Friedrich Biegler-König, University of applied sciences Bielefeld Germany (2000)
47. Hobza P, Havlas Z (2000) Chem Rev 100:4253
48. Marcus RA (1993) Rev Mod Phys 65:599
49. Marcus RA (1964) Annu Rev Phys Chem 15:155
50. Wen S, Li A, Song J, Deng W, Han K, Goddard WA III (2009) J Phys Chem B 113:8813
51. Yang XD, Wang LJ, Wang CL, Long W, Shuai ZG (2008) Chem Mater 20:3205
52. Troisi A, Orlandi G (2006) J Phys Chem A 110:4065
53. Lemaur V, Steel M, Beljonne D, Brédas JL, Cornil J (2005) J Am Chem Soc 127:6077
54. Hutchison GR, Ratner MA, Marks TJ (2005) J Am Chem Soc 127:2339
55. Köse ME, Mitchell WJ, Kopidakis N, Chang CH, Shaheen SE, Kim K, Rumbles GJ (2007) Am Chem Soc 129:14257
56. Cheung DL, Troisi A (2010) J Phys Chem C 114:20479
57. Martinelli NG, Idé J, Sánchez-Carrera RS, Coropceanu V, Brédas JL, Ducasse L, Castet F, Cornil J, Beljonne D (2010) J Phys Chem C 114:20678
58. McMahon DP, Trois A (2010) J Phys Chem Lett 1:941
59. Norton JE, Brédas JL (2008) J Am Chem Soc 130:12377
60. Köse ME, Long H, Kim K, Graf P, Ginley D (2010) J Phys Chem A 114:4388
61. Sakanoue K, Motoda M, Sugimoto M, Sakaki S (1999) J Phys Chem A 103:5551
62. Berlin YA, Hutchison GR, Rempala P, Ratner MA, Michl J (2003) J Phys Chem A 107:3970
63. Gruhn NE, da Silva Filho DA, Bill TG, Malagoli M, Coropceanu V, Kahn A, Brédas JL (2002) J Am Chem Soc 124:7918
64. Malagoli M, Brédas JL (2000) Chem Phys Lett 327:13
65. Lin BC, Cheng CP, You ZQ, Hsu CP (2005) J Am Chem Soc 127:66
66. Steiner T, Desiraju GR (1998) Chem Commun 891
67. Steiner T (2002) Angew Chem Int Ed 41:48
68. Amendola V, Esteban-Gómez D, Fabbrizzi L, Licchelli M (2006) Acc Chem Res 39:343
69. Sidorkin VF, Doronina EP, Chipanina NN, Aksamentova TN, Shainyan BA (2008) J Phys Chem A 112:6227
70. Nagaraju M, Narahari Sastry G (2011) J Mol Model 17:1801
71. Karabıyık H, Sevinçek R, Petek H, Aygün M (2011) J Mol Model 7:1295
72. Abramov YA (1997) Acta Crystallogr A 53:264
73. Bader RFW (1994) Atoms in molecules: a quantum theory. Clarendon Press, Oxford
74. Espinosa E, Molins E, Lecomte C (1998) Chem Phys Lett 285:170
75. Nakanishi W, Hayashi S, Narahara K (2008) J Phys Chem A 112:13593
76. Forés M, Duran M, Solà M, Adamowicz L (1999) J Phys Chem A 103:4413
77. Zhao GJ, Han KL (2012) Acc Chem Res 45:404
78. Zhao GJ, Liu JY, Zhou LC, Han KL (2007) J Phys Chem B 111:8940
79. Pearson RG (1985) J Am Chem Soc 107:6801
80. Start MS (1997) J Phys Chem A 101:8296